Electromagnetic Form Factors and Structure of the T_{bb} Tetraquark from Lattice QCD

Ivan Vujmilovic,[1,2,*] Sara Collins,[3,†] Luka Leskovec,[1,2,‡] and Sasa Prelovsek[1,2,§]
[1]Jožef Stefan Institute, Jamova 39, 1000 Ljubljana, Slovenia
[2]Faculty of Mathematics and Physics, University of Ljubljana, 1000 Ljubljana, Slovenia
[3]Institut für Theoretische Physik, Universität Regensburg, 93040 Regensburg, Germany

(Received 27 October 2025; revised 5 March 2026; accepted 12 March 2026; published 23 April 2026)

We present the first lattice QCD determination of the electromagnetic form factors of the exotic tetraquark $T_{bb}(bb\bar{u}\,\bar{d})$ with quantum numbers $I(J^P) = 0(1^+)$. The extracted form factors encode information about its internal structure, including the charge distribution and the magnetic dipole moments, determined separately for the light and heavy quarks. Our results provide evidence in favor of it being a bound state consisting of a compact heavy diquark $[bb]$ in a color-antitriplet with spin one and a light antidiquark $[\bar{u}\,\bar{d}]$ in a color-triplet with spin zero. The charge radius of T_{bb} is found to be significantly smaller than the combined charge radii of B and B^* mesons. These two comprise the lowest-lying threshold BB^* in the channel that we are considering, and their electric charge form factors are also determined. The computations were performed on a single ensemble, generated by the Coordinated Lattice Simulations effort, with $N_f = 2 + 1$ dynamical quarks and a lattice spacing of approximately $a \approx 0.064$ fm at the pion mass $m_\pi \approx 290$ MeV.

DOI: 10.1103/jnsy-5nhj

Introduction—Quantum chromodynamics (QCD), as an integral part of the standard model of particle physics, has achieved enormous success in explaining the existence of hadrons—mesons and baryons that are bound states or resonances. In a simple quark model picture these are built either from a single quark-antiquark pair $(\bar{q}_1 q_2)$ or three quarks $(q_1 q_2 q_3)$, respectively [1,2]. QCD also allows for the existence of more exotic states [3,4], e.g., tetraquarks $(\bar{q}_1 \bar{q}_2 q_3 q_4)$, pentaquarks $(q_1 \bar{q}_2 q_3 q_4 q_5)$, hybrid mesons $(\bar{q}_1 g q_2)$, or glueballlike mesons, the latter built mainly from gluons; many of these have been discovered experimentally [5–14]. Nevertheless the quest to determine how the exotic states populate the dense spectrum arising from QCD is one of the most active avenues of research in hadronic physics [15–18].

The as yet experimentally undiscovered doubly-bottom tetraquark, $T_{bb} = bb\bar{u}\,\bar{d}, I(J^P) = 0(1^+)$, has been particularly scrutinized as one the most promising candidates for an exotic QCD stable state [19–26]. State-of-the-art lattice studies find its mass to be significantly below the lowest compatible decay threshold, BB^*, in the $I = 0$ channel [20,27–34]. These studies are especially pertinent given the recent discovery of $T_{cc} = cc\bar{u}\,\bar{d}$ at LHCb [14] and the favorable prospects of observing $T_{bc} = bc\bar{u}\,\bar{d}$ [35,36], expected to lie slightly below the DB^* threshold [37–39]. Regarding T_{bb}, its production cross section at the LHC was determined to be a few nb [35]. Detection in exclusive decays seems unlikely [40], while there may be a possibility of observing T_{bb} in inclusive decays [40].

Information about the structure of composite particles, i.e., their spin, color, and orbital wave functions, are encoded in their form factors. They appear via Lorentz-covariant parametrizations of matrix elements $\mathcal{M} = \langle h_2(p_2,\lambda_2)|\hat{\jmath}(x=0)|h_1(p_1,\lambda_1)\rangle$, with $h_{1(2)}$ being single hadrons possessing momenta and helicities $p_{1(2)}$ and $\lambda_{1(2)}$ and the current $\hat{\jmath}$ representing the probe. Currently, almost all theoretically or experimentally studied form factors of QCD states involve the conventional states, e.g., pions [41–46], nucleons [47–52], kaons [44,46,53], and others (including transition and multiparticle form factors) [54–61].

Tetraquarks admit two color configurations that yield an $SU(3)$ singlet hadron [15,17,62]. One is the so-called *molecular structure* where the wave function is a product of two quark-antiquark pairs, both in definite color representations: $(\bar{q}_1 q_3)_1(\bar{q}_2 q_4)_1$, $(\bar{q}_1 q_4)_1(\bar{q}_2 q_3)_1$, and $(\bar{q}_1 q_3)_8(\bar{q}_2 q_4)_8$. The first two feature pairs of color-singlet hadrons interacting via residual color interactions. This structure prevails in nuclei composed of protons and neutrons and plays a prominent role for many tetraquark residing near meson-meson thresholds. The second possibility includes the *diquark-antidiquark structure*: $[\bar{q}_1 \bar{q}_2]_3[q_3 q_4]_{\bar{3}}$ or $[\bar{q}_1 \bar{q}_2]_{\bar{6}}[q_3 q_4]_6$. The former features a diquark in a color-antitriplet and an antidiquark in a color-triplet, while the latter

*Contact author: ivan.vujmilovic@ijs.si
†Contact author: sara.collins@ur.de
‡Contact author: luka.leskovec@ijs.si
§Contact author: sasa.prelovsek@ijs.si

is comprised of a color-sextet and a color-antisextet. These color wave functions are not linearly independent and can be related to each other [62,63].

In this work, we probe the structure of the doubly-bottom tetraquark T_{bb} by determining its electromagnetic form factors in lattice QCD. Its stability against strong decay guarantees that infinite-volume matrix elements $\langle T_{bb}|\hat{\jmath}|T_{bb}\rangle$ are directly accessible from the lattice and are not significantly polluted by finite-volume effects [64,65]. This feature sets the T_{bb} apart from all so-far discovered tetraquarks, which decay via strong interaction and therefore do not correspond to QCD asymptotic states. The T_{bb}, by contrast only decays weakly—like the pion, kaon, and other pseudoscalar hadrons. As such, it provides a unique opportunity to study the structure of a hadron, whose manifestly exotic character arises from its flavor content (two bottom quarks) and its electric charge.

$h \xrightarrow{\hat{\jmath}^\mu_{\mathrm{EM}}} h$ form factor decomposition—The matrix element linked to the electromagnetic (EM) composition of a hadron h is defined in the continuum as

$$\mathcal{M}^\mu_{\mathrm{EM}}(p_2,\lambda_2,p_1,\lambda_1) = \langle h(p_2,\lambda_2)|\hat{\jmath}^\mu_{\mathrm{EM,cont}}|h(p_1,\lambda_1)\rangle,$$
$$\hat{\jmath}^\mu_{\mathrm{EM,cont}} = \sum_q e_q \bar{q}\gamma^\mu q, \tag{1}$$

where e_q is the charge of quark q.

The decomposition of matrix element (1) is uniquely determined by the particle spin and the current $\hat{\jmath}$ [66]. For the same pseudoscalar in the initial and final states this renders a single form factor [67]

$$\mathcal{M}^\mu_{\mathrm{EM}} = (p_1+p_2)^\mu F_C(Q^2), \tag{2}$$

while for $J^P = 1^\pm$ particles this gives [68]

$$\begin{aligned}\mathcal{M}^\mu_{\mathrm{EM}} = &-(p_1+p_2)^\mu(\varepsilon_2^*\cdot\varepsilon_1)F_1(Q^2)\\ &-[(\varepsilon_2^*\cdot q)\varepsilon_1^\mu - (\varepsilon_1\cdot q)\varepsilon_2^{*\mu}]F_2(Q^2)\\ &+\frac{(\varepsilon_2^*\cdot q)(\varepsilon_1\cdot q)}{2m^2}(p_1+p_2)^\mu F_3(Q^2),\end{aligned} \tag{3}$$

with $Q^2 \equiv -q^2 = -(p_2-p_1)^2 > 0$ defined as the momentum transfer and $\varepsilon^{(*)}_{1(2)}$ as the polarization four vectors. $F_{C,1,2,3}(Q^2)$ are Lorentz scalars that are functions of Q^2. $F_{1,2,3}(Q^2)$ are further related to the charge, magnetic dipole, and electric quadrupole form factors, labeled by F_C, F_M, and $F_{\mathcal{Q}}$, respectively, via a linear transformation [68,69]

$$\begin{pmatrix} F_C(Q^2)\\ F_M(Q^2)\\ F_{\mathcal{Q}}(Q^2)\end{pmatrix} = \begin{pmatrix} 1+\frac{2}{3}\eta & -\frac{2}{3}\eta & \frac{2}{3}\eta(1+\eta)\\ 0 & 1 & 0\\ 1 & -1 & (1+\eta)\end{pmatrix}\begin{pmatrix} F_1(Q^2)\\ F_2(Q^2)\\ F_3(Q^2)\end{pmatrix}, \tag{4}$$

TABLE I. Hadron masses m_h and charge radii $\sqrt{\langle r_C^2\rangle}$. Columns r and t_+ show the resonances and multiparticle thresholds, respectively, that appear in the z-expansions.

h	m_h (GeV)	$\sqrt{\langle r_C^2\rangle}$ (fm)	r	t_+
T_{bb}	10.5765(98)	0.499(31)	ω	$(3m_\pi)^2$
B	5.3020(17)	0.692(21)	ρ	$(2m_\pi)^2$
B^*	5.3387(20)	0.698(23)	ρ	$(2m_\pi)^2$
π	0.28953(97)	0.652(20)	ρ	$(2m_\pi)^2$

with $\eta = (Q^2/4m^2)$. The normalization of the charge form factor at $Q^2 = 0$ is fixed to the total charge Z of the state in units of the elementary charge e_0, i.e., $F_C(Q^2=0) = Z$. The values of the electric quadrupole and the magnetic dipole form factors at $Q^2 = 0$ yield the values of the total electric quadrupole moment $\mathcal{Q} = (1/m^2)F_{\mathcal{Q}}(0)$ and the magnetic dipole moment $\mu = (1/2m)F_M(0)$ [70,71].

Lattice setup—We employ a single ensemble of gauge configurations (X253) with a hypervolume $N_L^3 \times N_T = 40^3 \times 128$ and lattice spacing $a = 0.06379(37)$ fm [72], generated by the Coordinated Lattice Simulations (CLS) effort [73]. This $N_f = 2+1$ ensemble features s and degenerate u/d quarks described by the nonperturbatively $O(a)$ improved Wilson action, resulting in a pion mass $m_\pi \approx 290$ MeV, listed in Table I. The bottom quark action is implemented with an anisotropic Clover action [74], tuned to reproduce the physical masses and continuum energy-momentum dispersions of B and B^* mesons on the ensemble [5].

The light and heavy EM currents,

$$\hat{\jmath}^\mu_{u/d} = Z^V_{u/d}\left(\frac{2}{3}\bar{u}\gamma^\mu u - \frac{1}{3}\bar{d}\gamma^\mu d\right), \quad \hat{\jmath}^\mu_b = Z^V_b\left(-\frac{1}{3}\bar{b}\gamma^\mu b\right),$$
$$\hat{\jmath}^\mu_{\mathrm{EM}} = \hat{\jmath}^\mu_{u/d} + \hat{\jmath}^\mu_b, \tag{5}$$

are nonperturbatively renormalized with factors $Z^V_{u/d}$ and Z^V_b determined from T_{bb} matrix elements to recover the infinite-volume and continuum normalization of the T_{bb} charge form factor, $F_C(0) = -1$. The b-quark action, its tuning, and current renormalization are described in Supplemental Material [75].

The desired matrix elements (1) for states $h = T_{bb}, B, B^*, \pi$ (generated by the interpolators $O_h^{(\dagger)}$ as detailed in [75]) were computed from three-point correlation functions $\mathcal{C}^\mu_3(\vec{p}_2,\vec{q},T;t)$, shown for T_{bb} in Fig. 1:

$$\begin{aligned}\mathcal{C}^\mu_3(\vec{p}_2,\vec{q},T;t) &= \langle\Omega|\mathcal{O}_h(\vec{p}_2,T)\hat{\jmath}^\mu_{\mathrm{EM}}(\vec{q},t)\mathcal{O}_h^\dagger(x=0)|\Omega\rangle\\ &= \sum_{n,m=0}^{\infty}\frac{\mathcal{Z}_n^{f*}\mathcal{Z}_m^i}{(2E_n^f)(2E_m^i)}\mathcal{M}^\mu_{nm}e^{-E_n^f(T-t)}e^{-E_m^i t}.\end{aligned} \tag{6}$$

Here $\vec{p}_2$ and $\vec{q} \equiv \vec{p}_2 - \vec{p}_1$ are momenta at the sink and the current, respectively, and T denotes the source-sink

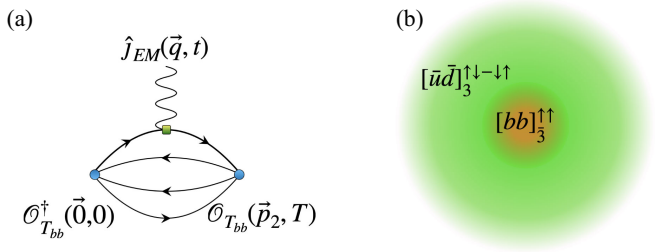

FIG. 1. (a) Example of a connected Wick contraction diagram generated by the T_{bb} three-point correlator (6). (b) Pictorial representation of the resulting distributions for light and heavy quarks.

temporal separation. The three-point function is decomposed in terms of initial states (i,m) and final states (f,n) in Euclidean time. The $\mathcal{Z}_a = \langle a|\mathcal{O}_h^{\dagger}|\Omega\rangle$ labels the overlap with the a th state, and E_a denotes its energy. In addition, operators $\mathcal{O}_h$ for $h = B^*, T_{bb}$ with nonzero spin are projected to the appropriate rows r and irreps Λ of subgroups of the octahedral group. In addition to the connected Wick contraction in Fig. 1(a) there might be in principle also a nonvanishing contribution of disconnected diagrams. The latter are typically found to be very small for EM currents (e.g. at most few percent [81] for nucleon) and we omit them in the current study.

To isolate the ground-state matrix element $\mathcal{M}^{\mu}_{00} \equiv \mathcal{M}^{\mu}$, we remove the zeroth-order dependence of the three-point correlator (6) on the ground-state overlap factors $\mathcal{Z}_0^{f(i)}$ and energies $E_0^{f(i)}$, obtained from the corresponding two-point correlators $C_2(\vec{p},t) = \langle\Omega|\mathcal{O}_h(\vec{p},t)\mathcal{O}_h^{\dagger}(0)|\Omega\rangle$. This is done by constructing the ratio $R_3^{\mu}(\vec{p},\vec{q},T;t)$,

$$R_3^{\mu}(\vec{p}_2,\vec{q},T;t) = \frac{(2E_0^f)(2E_0^i)}{\mathcal{Z}_0^{f*}\mathcal{Z}_0^i} e^{E_0^f(T-t)} e^{E_0^i t} C_3^{\mu}(\vec{p}_2,\vec{q},T;t), \tag{7}$$

defined in Eq. (28) of Supplemental Material of Ref. [61], that equals the desired matrix element, up to excited-state contamination. Two models are used in fits to data: a constant fit, assuming no contamination, or a model that also incorporates first-excited states [75]. To improve fit quality, we performed a weighted average of the ratios (7) over selected equivalent directions of the sink and source momenta that yield the same value of Q^2. The averaged data was simultaneously fitted for four source-sink separations $(T/a) = 12, 15, 18, 22$. The averaging procedure and plots showing representative fits are given in Supplemental Material [75].

Results—The extracted masses of T_{bb}, B, and B^*, listed in Table I, render a significant binding energy of the T_{bb} with respect to the BB^* threshold,

$$m_{T_{bb}} - (m_B + m_{B^*}) = -64(10)\ \text{MeV}, \tag{8}$$

at $m_\pi \approx 290$ MeV. This is in line with the large binding observed in previous studies, e.g., Refs. [20,23,27–32,34].

The EM form factors of hadrons $h = T_{bb}, B, B^*$, and π are shown in Figs. 2(a) and 3 for five values of Q^2. The latter plot also shows the individual EM form factors of the

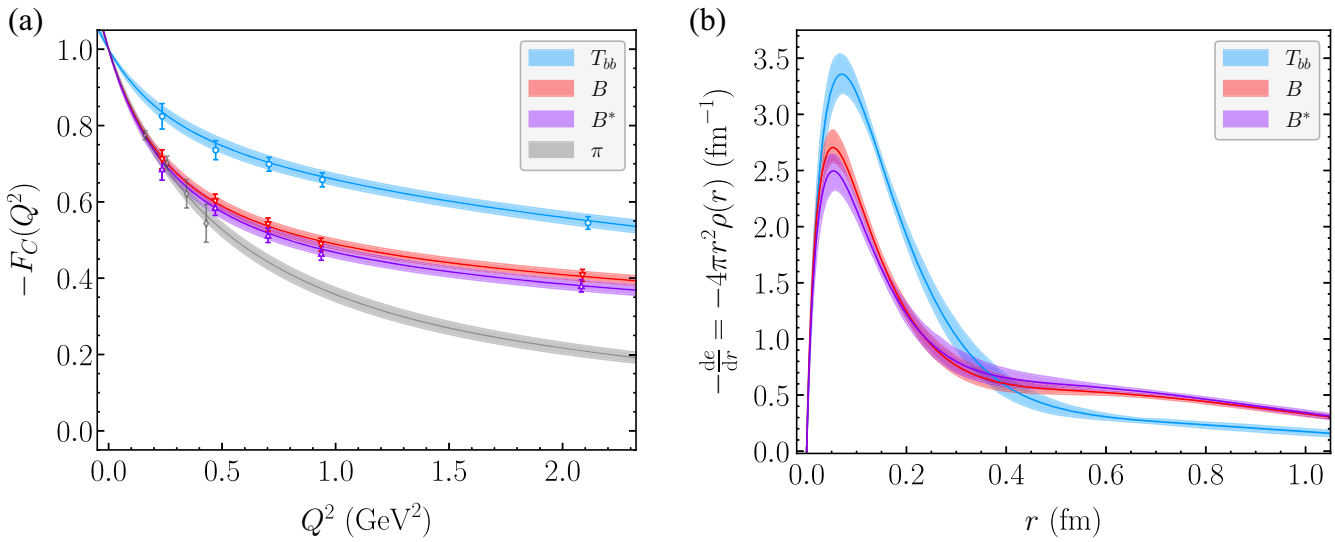

FIG. 2. (a) Charge form factors $F_C(Q^2)$ of hadrons $h = T_{bb}, B(b\bar{u}), B^*(b\bar{u}), \pi(d\bar{u})$, shown as a function of Q^2. Discrete markers show lattice data, and the bands represent z-expansion fits. Second order expansion [up to and including $n = 2$ in Eq. (9)] was used to parametrize T_{bb}, B, B^* electric form factors, while a first order expansion sufficed for an adequate parametrization of the pion form factor. (b) Position-space charge densities $\rho(r)$, represented in the form of $-(\mathrm{d}e/\mathrm{d}r) = -4\pi r^2\rho$, are related to the form factors via a Fourier transform. Negative values of charge form factors and distributions are shown, given that considered hadrons are negatively charged.

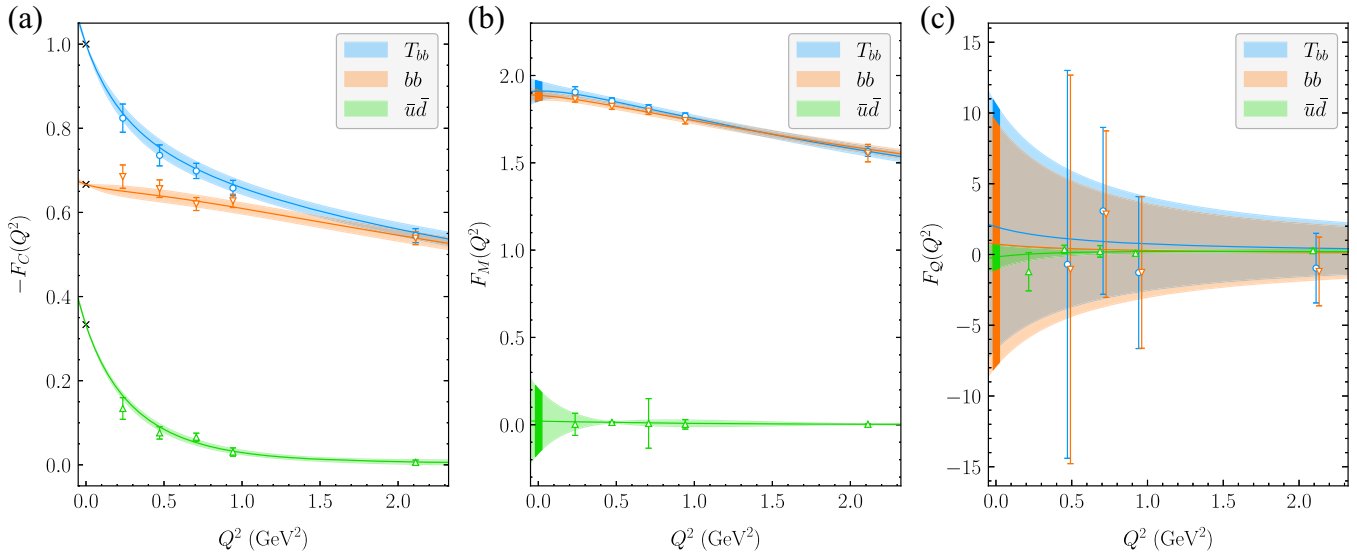

FIG. 3. Form factors of the T_{bb}. Each subfigure shows the total value of the form factors with separate contributions yielded by the light current $\hat{\jmath}^{\mu}_{u/d}$ and the heavy current $\hat{\jmath}^{\mu}_{b}$. The crosses in (a) mark values to which each of the charge form factors have been normalized at $Q^2 = 0$, and the shaded vertical bands in (b) and (c) indicate the values of magnetic dipole moments $2m_{T_{bb}}\mu$ and electric quadrupole moments $m^2_{T_{bb}}\mathcal{Q}$, respectively, also found in Table II. The points on the rightmost plot are slightly horizontally displaced for improved visibility.

light and heavy currents, extracted from matrix elements $\langle T_{bb}|\hat{\jmath}^{\mu}_{u/d}|T_{bb}\rangle$ and $\langle T_{bb}|\hat{\jmath}^{\mu}_{b}|T_{bb}\rangle$, respectively.

Continuous bands in Figs. 2 and 3 follow from parametrizing all form factors using the z-expansion [82–84] of the form

$$F(Q^2) = \frac{1}{1+\frac{Q^2}{m_r^2}}\sum_n a_n z^n(Q^2; t_+, t_0). \tag{9}$$

Here m_r is the mass of the closest resonance, and z is a variable that maps Q^2 to the unit disk,

$$z(Q^2; t_+, t_0) = \frac{\sqrt{t_+ + Q^2} - \sqrt{t_+ - t_0}}{\sqrt{t_+ + Q^2} + \sqrt{t_+ - t_0}}, \tag{10}$$

where t_+ is the squared mass of the nearest multiparticle threshold and t_0 is a tunable parameter. Table I lists the closest resonances and thresholds employed in fitting Eq. (9) to all form factors. The thresholds t_+ are evaluated at $m_\pi \approx 290$ MeV. As the ρ and ω resonance masses are not known on our ensemble, we use the PDG values and verify that the fits are robust when varying these masses within the range $m_{\omega,\rho} \in [750\ \text{MeV}, 900\ \text{MeV}]$. The coefficients a_n are fit parameters, and we truncate all expansions at order $n = 2$ or less, with their numerical values and that of t_0, given in Supplemental Material [75].

The electric charge and quadrupole form factors encode the information about the spatial charge distribution $\rho(\vec{r})$ [71] and consequently the charge radius $r_C \equiv \sqrt{\langle r_C^2\rangle} = \sqrt{6[\mathrm{d}F_C/\mathrm{d}Q^2](0)}$. We find that the quadrupole contribution in T_{bb} is negligible with respect to the monopole contribution, as shown in Fig. 3 of Supplemental Material [75]. The corresponding monopole of the spatial charge distribution is obtained via the Fourier transform, $\rho(r) = \int[\mathrm{d}^3q/(2\pi)^3]e^{i\vec{q}\cdot\vec{r}}F_C(|\vec{q}|^2)$, in the nonrelativistic limit, which is a good approximation for T_{bb}, B, and B^*. The resulting charge radius of the T_{bb}, 0.499(31) fm, is smaller than that of the B or B^* individually (listed in Table I) and significantly smaller than the sum of both, 1.390(31) fm. This is consistent with the T_{bb} charge density being concentrated at a smaller radius r than the charge densities of B or B^*; see Fig. 2(b). The compactness of the T_{bb} implies that the notion of a $B - B^*$ molecule is not meaningful and instead favors a compact diquark-antidiquark composition [33,85–87]. The B meson charge radius that we obtain is comparable to the values found in Refs. [88,89] and has been studied previously on the lattice through radial charge distributions in heavy-light mesons [90–92] with static heavy quarks.

TABLE II. Charge radii, magnetic dipole μ, and electric quadrupole moments $\mathcal{Q}$ of T_{bb} and the constituent (anti)diquarks. The same values are also shown with shaded bands at $Q^2 = 0$ in Figs. 3(b) and 3(c).

	T_{bb}	$[bb]$	$[\bar{u}\,\bar{d}]$
$\sqrt{\langle r_C^2\rangle}$ (fm)	0.499(31)	0.174(59)	0.511(14)
$2m_{T_{bb}}\cdot\mu$	1.912(57)	1.887(29)	0.02(18)
$m^2_{T_{bb}}\cdot\mathcal{Q}$	1.9(8.7)	0.6(8.8)	−0.18(86)

The diquark-antidiquark structure is further supported by investigating the charge distributions of light and heavy (anti)diquarks separately in Fig. 3(a). We find that the $[bb]$ diquark component of the total charge form factor has significantly weaker Q^2 dependence than the antidiquark $[\bar{u}\,\bar{d}]$ component, indicating that the diquark is more localized than the antidiquark; see Table II. This suggests that the structure with a very compact heavy diquark and a relatively spatially extended antidiquark is responsible for the large binding energy of the tetraquark, compatible with some quark model studies [22,62,85,86,93–95].

Motivated by our findings, we assume that the T_{bb} state vector in the QCD Hilbert space can be expanded in the diquark-antidiquark basis with compatible quantum numbers, in line with quark models applied to QCD exotics. Each diquark-antidiquark state is factorized into three components (orbital, spin, and color) [22,62]:

$$\{[bb]^{l_{bb},s_{bb}}_{\bar{c}}[\bar{u}\,\bar{d}]^{I=0,l_{\bar{u}\bar{d}},s_{\bar{u}\bar{d}}}_{c}\}^{J^P=1^+}_{l_{12}}, \tag{11}$$

where l_{bb} and $l_{\bar{u}\bar{d}}$ denote the relative orbital angular momenta in the diquark and antidiquark, respectively, and $s_{bb}, s_{\bar{u}\bar{d}} = 0,\ 1$ are their corresponding spins. l_{12} is the relative angular momentum between the diquark and the antidiquark, and $c = 3, \bar{6}$ are color configurations, as discussed in the introduction. The values introduced in Eq. (11) are subject to the constraints imposed by the T_{bb} quantum numbers $I(J^P) = 0(1^+)$ and the Pauli principle, ensuring that the total T_{bb} state is antisymmetric with respect to the permutations of the b quarks or the light antiquarks in the isospin limit. Accounting for this yields three relations [22,93]:

$$\begin{aligned}&(a)\ (-1)^{s_{bb}+l_{bb}+c} = 1, \quad (b)\ (-1)^{s_{\bar{u}\bar{d}}+l_{\bar{u}\bar{d}}+c} = -1,\\ &(-1)^{l_{bb}+l_{\bar{u}\bar{d}}+l_{12}} = 1 \xrightarrow{(a),(b)} (-1)^{s_{bb}+s_{\bar{u}\bar{d}}+l_{12}} = -1,\end{aligned} \tag{12}$$

where the first row follows from the Pauli principle and the second ensures positive parity.

Our results for the electric quadrupole form factors are consistent with zero, as presented in Fig. 3(c) and Table II, given the present level of accuracy. This applies to the total value and separate diquark and antidiquark contributions. It indicates that the S-wave $(l_{bb} = l_{\bar{u}\bar{d}} = l_{12} = 0)$ components dominate in the relative wave functions within the diquark, antidiquark, and total system [96,97]. The magnetic dipole moment of the T_{bb},

$$\mu_{T_{bb}} = \langle T_{bb}|\sum_{q=u,d,b}\frac{e_q}{2m_q}(\hat{l}_q + g_q\hat{s}_q)|T_{bb}\rangle = \frac{F_M(0)}{2m_{T_{bb}}}, \tag{13}$$

is determined from the value of the magnetic dipole form factor F_M at $Q^2 = 0$. It is nonzero and almost completely saturated by the contribution from the heavy quarks as seen in Fig. 3(b), implying that the light quarks dominantly form a spin singlet state, while the heavy quarks are in a spin triplet state,

$$s_{\bar{u}\bar{d}} = 0, \quad s_{bb} = 1. \tag{14}$$

Note that T_{bb} with molecular structure $B - B^*$ would not render a spin correlation within two light quarks or correlation within two heavy quarks, disfavoring the molecular structure. Taking into account the orbital and spin quantum numbers, Eq. (12) restricts the diquark-antidiquark to be in an antisymmetric color triplet-antitriplet configuration, i.e., $c = 3$. This uniquely determines the T_{bb} state in QCD Hilbert space to be

$$|T_{bb}\rangle = \{[bb]^{l_{bb}=0,s_{bb}=1}_{\bar{3}}[\bar{u}\,\bar{d}]^{I=0,l_{\bar{u}\bar{d}}=0,s_{\bar{u}\bar{d}}=0}_{3}\}^{J^P=1^+}_{l_{12}=0}, \tag{15}$$

which is the simplest and the dominant configuration not in tension with our lattice results. Result (15) is graphically summarized in Fig. 1(b).

The identified structure features the "good" light antidiquark [3], in which the attraction between two quarks increases with decreasing $m_{u/d}$ [98]; therefore, the dominance of this structure is expected to pertain also at the physical light quark masses. We also expect that our findings, including the assignment of the quantum numbers in Eq. (15), are not significantly affected by finite-volume or lattice spacing effects. Future lattice QCD studies at smaller pion masses and lattice spacings, as well as larger volumes, are desirable to confirm this.

Conclusions—In this work we have presented the first lattice QCD calculation of electromagnetic form factors of an exotic tetraquark T_{bb}. All computations were done on one CLS ensemble at the pion mass $m_\pi \approx 290$ MeV, at which we observe T_{bb} to be a strongly stable state with a binding energy $m_{T_{bb}} - (m_B + m_{B^*}) = -64(10)$ MeV.

By probing T_{bb} with the electromagnetic light and heavy currents, we extracted three form factors that reveal three components of its structure: the electric charge distribution, the magnetic dipole moment, and the electric quadrupole moment. Flavor decompositions of all form factors were determined from the respective matrix elements.

These observables were combined with constraints from the Pauli principle. We have shown that, within the precision of our data, the T_{bb} is a compact bound state consisting of a heavy diquark $[bb]$ in a color-antitriplet with spin one, and a light antidiquark $[\bar{u}\,\bar{d}]$ in a color-triplet with spin zero. The structure of T_{bb} is therefore rather unique as it differs from a molecular structure that dominates in many tetraquarks near meson-meson thresholds and prevails in nuclei composed of protons and neutrons.

In the future, it would be valuable to investigate the structure of the Λ_b and Ξ_{bb} baryons, which might be related to that of T_{bb} and the B meson, respectively, via the symmetry between the heavy diquark and the heavy antiquark. Similarly, determining the EM form factors of T_{bc} and eventually T_{cc} would shed light on the heavy quark

mass dependence of the internal configuration of double heavy tetraquarks.

Software packages QDP-JIT [99] and Chroma [100] were used for computing the Wick contractions and inverting the heavy quark Dirac operator, and the QUDA multigrid solver was employed for the light quark Dirac operator inversions [101].

Acknowledgments—We thank M. Padmanath for valuable discussions during the early stages of the project, R. J. Hudspith for insights regarding the heavy-quark tuning and Jeremy Green for valuable discussion related to disconnected diagrams. We thank our colleagues who are part of CLS for their joint effort in the generation of gauge configurations that were employed in lattice simulations for this study. The authors gratefully acknowledge the HPC RIVR consortium [102] and EuroHPC JU [103] for funding this research by providing computing resources of the HPC system Vega at the Institute of Information Science [104], in particular the project QCD on Vega (S24O01-37 and 525002-11). The authors also acknowledge the scientific support and HPC resources provided by the Erlangen National High Performance Computing Center (NHR@FAU) of the Friedrich-Alexander-Universität Erlangen-Nürnberg (FAU) under the NHR Project No. b124da. NHR funding is provided by federal and Bavarian state authorities. NHR@FAU hardware is partially funded by the German Research Foundation (DFG)—440719683. The work of I. V. is supported by the Slovenian Research Agency (core Funding. No. PR-12831,P1-0035, N1-0360), while the work of L. L. and S. P. is supported by the Slovenian Research Agency (core Funding No. P1-0035, N1-0360, J1-70036, J1-3034).

Data availability—The data that support the findings of this article are openly available [105], embargo periods may apply.

[1] M. Gell-Mann, A schematic model of baryons and mesons, Phys. Lett. **8**, 214 (1964).
[2] G. Zweig, An SU(3) Model for Strong Interaction Symmetry and Its Breaking. Version 2 (Hadronic Press; Nonantum, 1964) pp. 22–101.
[3] R. L. Jaffe, Exotica, Phys. Rep. **409**, 1 (2005).
[4] R. F. Lebed, R. E. Mitchell, and E. S. Swanson, Heavy-quark QCD exotica, Prog. Part. Nucl. Phys. **93**, 143 (2017).
[5] S. Navas *et al.* (Particle Data Group), Review of particle physics, Phys. Rev. D **110**, 030001 (2024).
[6] S. K. Choi *et al.* (Belle Collaboration), Observation of a narrow charmonium-like state in exclusive $B^{\pm} \to K^{\pm}\pi^{+}\pi^{-}J/\psi$ decays, Phys. Rev. Lett. **91**, 262001 (2003).
[7] S. K. Choi *et al.* (Belle Collaboration), Observation of a resonance-like structure in the $\pi^{\pm}\psi'$ mass distribution in exclusive $B \to K\pi^{\pm}\psi'$ decays, Phys. Rev. Lett. **100**, 142001 (2008).
[8] M. Ablikim *et al.* (BESIII Collaboration), Observation of a charged charmoniumlike structure in $e^{+}e^{-} \to \pi^{+}\pi^{-}J/\psi$ at $\sqrt{s} = 4.26$ GeV, Phys. Rev. Lett. **110**, 252001 (2013).
[9] B. Aubert *et al.* (*BABAR* Collaboration), Observation of a broad structure in the $\pi^{+}\pi^{-}J/\psi$ mass spectrum around 4.26-GeV/c^2, Phys. Rev. Lett. **95**, 142001 (2005).
[10] R. Aaij *et al.* (LHCb Collaboration), Observation of $J/\psi p$ resonances consistent with pentaquark States in $\Lambda_b^0 \to J/\psi K^{-} p$ decays, Phys. Rev. Lett. **115**, 072001 (2015).
[11] R. Aaij *et al.* (LHCb Collaboration), Observation of a narrow pentaquark state, $P_c(4312)^{+}$, and of two-peak structure of the $P_c(4450)^{+}$, Phys. Rev. Lett. **122**, 222001 (2019).
[12] T. Aaltonen *et al.* (CDF Collaboration), Evidence for a narrow near-threshold structure in the $J/\psi\phi$ mass spectrum in $B^{+} \to J/\psi\phi K^{+}$ decays, Phys. Rev. Lett. **102**, 242002 (2009).
[13] R. Aaij *et al.* (LHCb Collaboration), Observation of $J/\psi\phi$ structures consistent with exotic states from amplitude analysis of $B^{+} \to J/\psi\phi K^{+}$ decays, Phys. Rev. Lett. **118**, 022003 (2017).
[14] R. Aaij *et al.* (LHCb Collaboration), Observation of an exotic narrow doubly charmed tetraquark, Nat. Phys. **18**, 751 (2022).
[15] P. Bicudo, Tetraquarks and pentaquarks in lattice QCD with light and heavy quarks, Phys. Rep. **1039**, 1 (2023).
[16] A. Francis, Lattice perspectives on doubly heavy tetraquarks, Prog. Part. Nucl. Phys. **140**, 104143 (2025).
[17] N. Brambilla, S. Eidelman, C. Hanhart, A. Nefediev, C.-P. Shen, C. E. Thomas, A. Vairo, and C.-Z. Yuan, The *XYZ* states: Experimental and theoretical status and perspectives, Phys. Rep. **873**, 1 (2020).
[18] J. Bulava *et al.*, Hadron spectroscopy with Lattice QCD, in *Snowmass 2021* (2022).
[19] E. J. Eichten and C. Quigg, Heavy-quark symmetry implies stable heavy tetraquark mesons $Q_i Q_j \bar{q}_k \bar{q}_l$, Phys. Rev. Lett. **119**, 202002 (2017).
[20] P. Bicudo and M. Wagner (European Twisted Mass Collaboration), Lattice QCD signal for a bottom-bottom tetraquark, Phys. Rev. D **87**, 114511 (2013).
[21] M. Karliner and J. L. Rosner, Discovery of the doubly charmed Ξ_{cc} baryon implies a stable $bb\bar{u}\bar{d}$ tetraquark, Phys. Rev. Lett. **119**, 202001 (2017).
[22] J. Vijande, A. Valcarce, and N. Barnea, Exotic meson-meson molecules and compact four-quark states, Phys. Rev. D **79**, 074010 (2009).
[23] N. Brambilla, A. Mohapatra, T. Scirpa, and A. Vairo, Nature of $\chi c1(3872)$ and $Tcc + (3875)$, Phys. Rev. Lett. **135**, 131902 (2025).
[24] J. Hoffer, G. Eichmann, and C. S. Fischer, Structure of open-flavor four-quark states in the charm and bottom region, Phys. Rev. D **111**, 054028 (2025).
[25] D. Janc and M. Rosina, The $T_{cc} = DD^{*}$ molecular state, Few-Body Syst. **35**, 175 (2004).
[26] L. Maiani, A. Pilloni, A. D. Polosa, and V. Riquer, Doubly heavy tetraquarks in the Born-Oppenheimer approximation, Phys. Lett. B **836**, 137624 (2023).

[27] R. J. Hudspith and D. Mohler, Exotic tetraquark states with two $\bar{b}$ quarks and $J^P = 0^+$ and 1^+ B_s states in a non-perturbatively tuned lattice NRQCD setup, Phys. Rev. D **107**, 114510 (2023).

[28] L. Leskovec, S. Meinel, M. Pflaumer, and M. Wagner, Lattice qcd investigation of a doubly-bottom $\bar{b}\,\bar{b}\,ud$ tetraquark with quantum numbers $i(J^P) = 0(1^+)$, Phys. Rev. D **100**, 014503 (2019).

[29] B. Colquhoun, A. Francis, R. J. Hudspith, R. Lewis, K. Maltman, and W. G. Parrott, Improved analysis of strong-interaction-stable doubly bottom tetraquarks on the lattice, Phys. Rev. D **110**, 094503 (2024).

[30] C. Alexandrou, J. Finkenrath, T. Leontiou, S. Meinel, M. Pflaumer, and M. Wagner, $\bar{b}\,\bar{b}\,ud$ and $\bar{b}\,\bar{b}\,us$ tetraquarks from lattice QCD using symmetric correlation matrices with both local and scattering interpolating operators, Phys. Rev. D **110**, 054510 (2024).

[31] T. Aoki, S. Aoki, and T. Inoue, Lattice study on a tetraquark state T_{bb} in the HAL QCD method, Phys. Rev. D **108**, 054502 (2023).

[32] P. Junnarkar, N. Mathur, and M. Padmanath, Study of doubly heavy tetraquarks in lattice QCD, Phys. Rev. D **99**, 034507 (2019).

[33] S. Prelovsek, E. Ortiz-Pacheco, S. Collins, L. Leskovec, M. Padmanath, and I. Vujmilovic, Doubly heavy tetraquarks from lattice QCD: Incorporating diquark-antidiquark operators and the left-hand cut, Phys. Rev. D **112**, 014507 (2025).

[34] B. S. Tripathy, N. Mathur, and M. Padmanath, bbu^-d^- and bsu^-d^- tetraquarks from lattice QCD using two-meson and diquark-antidiquark variational basis, Phys. Rev. D **111**, 114504 (2025).

[35] A. Ali, Q. Qin, and W. Wang, Discovery potential of stable and near-threshold doubly heavy tetraquarks at the LHC, Phys. Lett. B **785**, 605 (2018).

[36] Ivan Polyakov, LHCb mini-workshop: T_{bc} (2023).

[37] C. Alexandrou, J. Finkenrath, T. Leontiou, S. Meinel, M. Pflaumer, and M. Wagner, Shallow bound states and hints for broad resonances with quark content b^-c^-ud in $B\text{-}D^-$ and $B^*\text{-}D^-$ scattering from lattice QCD, Phys. Rev. Lett. **132**, 151902 (2024).

[38] A. Radhakrishnan, M. Padmanath, and N. Mathur, Study of the isoscalar scalar bcu^-d^- tetraquark T_{bc} with lattice QCD, Phys. Rev. D **110**, 034506 (2024).

[39] M. Padmanath, A. Radhakrishnan, and N. Mathur, Bound isoscalar axial-vector bcu^-d^- tetraquark T_{bc} from lattice QCD using two-meson and diquark-antidiquark variational basis, Phys. Rev. Lett. **132**, 201902 (2024).

[40] T. Gershon and A. Poluektov, Displaced B_c^- mesons as an inclusive signature of weakly decaying double beauty hadrons, J. High Energy Phys. 01 (2019) 019.

[41] V. Tadevosyan *et al.* (Jefferson Lab F(pi) Collaboration), Determination of the pion charge form-factor for $Q^2 = 0.60$–$1.60\ GeV^2$, Phys. Rev. C **75**, 055205 (2007).

[42] G. M. Huber *et al.* (Jefferson Lab Collaboration), Charged pion form-factor between $Q^2 = 0.60$ and $2.45\ GeV^2$. II. Determination of, and results for, the pion form-factor, Phys. Rev. C **78**, 045203 (2008).

[43] X. Gao, N. Karthik, S. Mukherjee, P. Petreczky, S. Syritsyn, and Y. Zhao, Pion form factor and charge radius from lattice QCD at the physical point, Phys. Rev. D **104**, 114515 (2021).

[44] C. Alexandrou, S. Bacchio, I. Cloët, M. Constantinou, J. Delmar, K. Hadjiyiannakou, G. Koutsou, C. Lauer, and A. Vaquero (ETM Collaboration), Scalar, vector, and tensor form factors for the pion and kaon from lattice QCD, Phys. Rev. D **105**, 054502 (2022).

[45] F. V. Ignatov *et al.* (CMD-3 Collaboration), Measurement of the pion form factor with CMD-3 detector and its implication to the hadronic contribution to muon (g-2), Phys. Rev. Lett. **132**, 231903 (2024).

[46] F. G. Ortega-Gama, J. J. Dudek, and R. G. Edwards (for the Hadron Spectrum Collaboration), Timelike meson form factors beyond the elastic region from lattice QCD, Phys. Rev. D **110**, 094505 (2024).

[47] C. Alexandrou, S. Bacchio, M. Constantinou, J. Finkenrath, K. Hadjiyiannakou, K. Jansen, G. Koutsou, and A. V. Aviles-Casco, Proton and neutron electromagnetic form factors from lattice QCD, Phys. Rev. D **100**, 014509 (2019).

[48] D. Djukanovic, G. von Hippel, H. B. Meyer, K. Ottnad, M. Salg, and H. Wittig, Electromagnetic form factors of the nucleon from $N_f = 2 + 1$ lattice QCD, Phys. Rev. D **109**, 094510 (2024).

[49] S. Park, R. Gupta, B. Yoon, S. Mondal, T. Bhattacharya, Y.-C. Jang, B. Joó, and F. Winter (Nucleon Matrix Elements (NME) Collaboration), Precision nucleon charges and form factors using $(2 + 1)$-flavor lattice QCD, Phys. Rev. D **105**, 054505 (2022).

[50] C. Chen, C. S. Fischer, C. D. Roberts, and J. Segovia, Nucleon axial-vector and pseudoscalar form factors and PCAC relations, Phys. Rev. D **105**, 094022 (2022).

[51] M. K. Jones *et al.* (Jefferson Lab Hall A Collaboration), G_{Ep}/G_{Mp} ratio by polarization transfer in $\vec{e}p \to e\vec{p}$, Phys. Rev. Lett. **84**, 1398 (2000).

[52] S. N. Santiesteban *et al.* (Jefferson Lab Hall A Collaboration), Novel measurement of the neutron magnetic form factor from $A = 3$ mirror nuclei, Phys. Rev. Lett. **132**, 162501 (2024).

[53] M. Carmignotto *et al.*, Separated kaon electroproduction cross section and the kaon form factor from 6 GeV JLab data, Phys. Rev. C **97**, 025204 (2018).

[54] C. Alexandrou, G. Koutsou, H. Neff, J. W. Negele, W. Schroers, and A. Tsapalis, Nucleon to delta electromagnetic transition form factors in lattice QCD, Phys. Rev. D **77**, 085012 (2008).

[55] D. C. Hackett, D. A. Pefkou, and P. E. Shanahan, Gravitational form factors of the proton from lattice QCD, Phys. Rev. Lett. **132**, 251904 (2024).

[56] J. Delaney, C. E. Thomas, and S. M. Ryan (Hadron Spectrum Collaboration), Radiative transitions in charmonium from lattice QCD, J. High Energy Phys. 05 (2024) 230.

[57] J. J. Dudek, R. G. Edwards, and D. G. Richards, Radiative transitions in charmonium from lattice QCD, Phys. Rev. D **73**, 074507 (2006).

[58] R. Abbott, D. C. Hackett, D. A. Pefkou, F. Romero-López, and P. E. Shanahan, Lattice evidence that scalar glueballs are small, arXiv:2508.21821.

[59] G. Ramalho, Electromagnetic form factors of the Ω^- baryon in the spacelike and timelike regions, Phys. Rev. D **103**, 074018 (2021).

[60] A. J. Buchmann, E. Hernández, and A. Faessler, Electromagnetic properties of the $\Delta(1232)$, Phys. Rev. C **55**, 448 (1997).

[61] L. Leskovec, S. Meinel, M. Petschlies, J. Negele, S. Paul, and A. Pochinsky, $b \to \rho \ell \bar{\nu}$ resonance form factors from $b \to \pi\pi \ell \bar{\nu}$ in lattice QCD, Phys. Rev. Lett. **134**, 161901 (2025).

[62] Y. Tan, X. Liu, X. Chen, Y. Wu, H. Huang, and J. Ping, Equivalence among color-singlet, color-octet, and diquark structures in a chiral quark model, Phys. Rev. D **109**, 076026 (2024).

[63] M. Padmanath, C. B. Lang, and S. Prelovsek, $x(3872)$ and $y(4140)$ using diquark-antidiquark operators with lattice QCD, Phys. Rev. D **92**, 034501 (2015).

[64] R. A. Briceño and M. T. Hansen, Relativistic, model-independent, multichannel $2 \to 2$ transition amplitudes in a finite volume, Phys. Rev. D **94**, 013008 (2016).

[65] A. Baroni, R. A. Briceño, M. T. Hansen, and F. G. Ortega-Gama, Form factors of two-hadron states from a covariant finite-volume formalism, Phys. Rev. D **100**, 034511 (2019).

[66] L. Durand, P. C. DeCelles, and R. B. Marr, Lorentz invariance and the kinematic structure of vertex functions, Phys. Rev. **126**, 1882 (1962).

[67] A. Khodjamirian, *Hadron Form Factors* (CRC Press, Boca Raton, 2020).

[68] R. G. Arnold, C. E. Carlson, and F. Gross, Polarization transfer in elastic electron scattering from nucleons and deuterons, Phys. Rev. C **23**, 363 (1981).

[69] F. Gross, Relativistic calculation of the deuteron electromagnetic form factor. II, Phys. Rev. **136**, B140 (1964).

[70] H. Haberzettl, Model-independent form-factor constraints for electromagnetic spin-1 currents, Phys. Rev. D **100**, 036008 (2019).

[71] C. Lorce, Electromagnetic properties for arbitrary spin particles. Part 1. Electromagnetic current and multipole decomposition, arXiv:0901.4199.

[72] G. S. Bali, S. Collins, P. Georg, D. Jenkins, P. Korcyl, A. Schäfer, E. E. Scholz, J. Simeth, W. Söldner, and S. Weishäupl (RQCD Collaboration), Scale setting and the light baryon spectrum in $N_f = 2 + 1$ QCD with Wilson fermions, J. High Energy Phys. 05 (2023) 035.

[73] M. Bruno *et al.*, Simulation of QCD with $N_f = 2 + 1$ flavors of non-perturbatively improved Wilson fermions, J. High Energy Phys. 02 (2015) 043.

[74] P. Chen, Heavy quarks on anisotropic lattices: The charmonium spectrum, Phys. Rev. D **64**, 034509 (2001).

[75] See Supplemental Material at http://link.aps.org/supplemental/10.1103/jnsy-5nhj for more details about the lattice setup and subsequent analysis of the spectrum and matrix elements. Refs. [76–80] are additionally cited in the Supplemental Material.

[76] J. J. Dudek, R. G. Edwards, M. J. Peardon, D. G. Richards, and C. E. Thomas, Toward the excited meson spectrum of dynamical QCD, Phys. Rev. D **82**, 034508 (2010).

[77] V. Bernard, M. Lage, U.-G. Meissner, and A. Rusetsky, Resonance properties from the finite-volume energy spectrum, J. High Energy Phys. 08 (2008) 024.

[78] M. Albanese *et al.* (APE Collaboration), Glueball masses and string tension in lattice QCD, Phys. Lett. B **192**, 163 (1987).

[79] C. Morningstar and M. Peardon, Analytic smearing of SU(3) link variables in lattice QCD, Phys. Rev. D **69**, 054501 (2004).

[80] A. X. El-Khadra, A. S. Kronfeld, and P. B. Mackenzie, Massive fermions in lattice gauge theory, Phys. Rev. D **55**, 3933 (1997).

[81] C. Alexandrou, M. Constantinou, K. Hadjiyiannakou *et al.*, Strange nucleon electromagnetic form factors from lattice QCD, Phys. Rev. D **97**, 094504 (2018).

[82] C. G. Boyd, B. Grinstein, and R. F. Lebed, Constraints on form-factors for exclusive semileptonic heavy to light meson decays, Phys. Rev. Lett. **74**, 4603 (1995).

[83] C. G. Boyd and M. J. Savage, Analyticity, shapes of semileptonic form-factors, and anti-B− > pi lepton anti-neutrino, Phys. Rev. D **56**, 303 (1997).

[84] C. Bourrely, I. Caprini, and L. Lellouch, Model-independent description of B− > pi l nu decays and a determination of −V(ub)−, Phys. Rev. D **79**, 013008 (2009); **82**, 099902(E) (2010).

[85] K.-K. Zhang, W.-X. Zhang, and D. Jia, Systematics of doubly heavy strange and nonstrange tetraquarks, Phys. Rev. D **112**, 054008 (2025).

[86] J.-B. Cheng, S.-Y. Li, Y.-R. Liu, Z.-G. Si, and T. Yao, Double-heavy tetraquark states with heavy diquark-antiquark symmetry, Chin. Phys. C **45**, 043102 (2021).

[87] S. H. Lee and S. Yasui, Stable multiquark states with heavy quarks in a diquark model, Eur. Phys. J. C **64**, 283 (2009).

[88] C.-W. Hwang, Charge radii of light and heavy mesons, Eur. Phys. J. C **23**, 585 (2002).

[89] A. S. Miramontes, J. Papavassiliou, and J. M. Pawlowski, Electromagnetic properties of heavy-light mesons, Eur. Phys. J. C **85**, 1390 (2025).

[90] D. Becirevic, E. Chang, and A. Le Yaouanc, On internal structure of the heavy-light mesons, Phys. Rev. D **80**, 034504 (2009).

[91] A. M. Green, J. Koponen, P. Pennanen, and C. Michael (UKQCD Collaboration), Charge and matter radial distributions of heavy-light mesons calculated on a lattice, Phys. Rev. D **65**, 014512 (2001).

[92] J. Koponen, A. M. Green, C. Michael, and P. Pennanen (UKQCD Collaboration), The radial distributions of a heavy light meson on a lattice, Nucl. Phys. B, Proc. Suppl. **119**, 638 (2003).

[93] E. Santopinto and G. Galatà, Spectroscopy of tetraquark states, Phys. Rev. C **75**, 045206 (2007).

[94] S.-Q. Luo, K. Chen, X. Liu, Y.-R. Liu, and S.-L. Zhu, Exotic tetraquark states with the $qq\bar{Q}\,\bar{Q}$ configuration, Eur. Phys. J. C **77**, 709 (2017).

[95] G. Yang, J. Ping, and J. Segovia, Double-heavy tetraquarks, Phys. Rev. D **101**, 014001 (2020).

[96] R. D. Amado, The deuteron D state revisited, Comments Nucl. Part. Phys. **10**, 131 (1981).

[97] M. Bashkanov, D. P. Watts, and A. Pastore, Electromagnetic properties of the $d^*(2380)$ hexaquark, Phys. Rev. C **100**, 012201 (2019).

[98] A. Francis, P. de Forcrand, R. Lewis, and K. Maltman, Diquark properties from full QCD lattice simulations, J. High Energy Phys. 05 (2022) 062.
[99] F. T. Winter, QDP-JIT/PTX: A QDP ++ Implementation for CUDA-Enabled GPUs, Proc. Sci. LATTICE2013 (**2014**) 042.
[100] R. G. Edwards and B. Joo (SciDAC, LHPC, and UKQCD Collaborations), The chroma software system for lattice QCD, Nucl. Phys. B, Proc. Suppl. **140**, 832 (2005).
[101] M. A. Clark, R. Babich, K. Barros, R. C. Brower, and C. Rebbi (QUDA Collaboration), Solving Lattice QCD systems of equations using mixed precision solvers on GPUs, Comput. Phys. Commun. **181**, 1517 (2010).
[102] https://www.hpc-rivr.si.
[103] https://eurohpc-ju.europa.eu.
[104] https://www.izum.si/en/home.
[105] Central values and the covariance matrices of form factors shown in this work can be found at http://www-f1.ijs.si/ sa sa/available-lattice-data/form-factors-Tbb.txt.